nanomaterials

MDPI

Article

Improving the NO_2 Gas Sensing Performances at Room Temperature Based on TiO_2 NTs/rGO Heterojunction Nanocomposites

Yan Ling [1], Yunjiang Yu [1], Canxin Tian [1,2] and Changwei Zou [1,2,*]

[1] Key Laboratory of Advanced Coating and Surface Engineering, Lingnan Normal University, Zhanjiang 524048, China; lingyan@lingnan.edu.cn (Y.L.); sidui@lingnan.edu.cn (Y.Y.); cxtian@lingnan.edu.cn (C.T.)
[2] Research Center for Engineering Technology in Surface Strengthening of Guangdong Province, Lingnan Normal University, Zhanjiang 524048, China
* Correspondence: zoucw@lingnan.edu.cn; Tel./Fax: +86-759-3183260

Abstract: The development of energy-efficient, sensitive, and reliable gas sensors for monitoring NO_2 concentrations has garnered considerable attention in recent years. In this manuscript, TiO_2 nanotube arrays/reduced graphene oxide nanocomposites with varying rGO contents (TiO_2 NTs/rGO) were synthesized via a two-step method for room temperature NO_2 gas detection. From SEM and TEM images, it is evident that the rGO sheets not only partially surround the TiO_2 nanotubes but also establish interconnection bridges between adjacent nanotubes, which is anticipated to enhance electron–hole separation by facilitating electron transfer. The optimized TiO_2 NTs/rGO sensor demonstrated a sensitive response of 19.1 to 1 ppm of NO_2, a 5.26-fold improvement over the undoped TiO_2 sensor. Additionally, rGO doping significantly enhanced the sensor's response/recovery times, reducing them from 24 s/42 s to 18 s/33 s with just 1 wt.% rGO. These enhancements are attributed to the increased specific surface area, higher concentration of chemisorbed oxygen species, and the formation of p-n heterojunctions between TiO_2 and rGO within the nanocomposites. This study provides valuable insights for the development of TiO_2/graphene-based gas sensors for detecting oxidizing gases at room temperature.

Keywords: TiO_2 nanotubes; reduced graphene oxide; NO_2 gas sensing; nanocomposites; room temperature sensors

check for updates

Citation: Ling, Y.; Yu, Y.; Tian, C.; Zou, C. Improving the NO_2 Gas Sensing Performances at Room Temperature Based on TiO_2 NTs/rGO Heterojunction Nanocomposites. *Nanomaterials* **2024**, *14*, 1844. https://doi.org/10.3390/nano14221844

Academic Editors: Manuel António Peralta Evaristo and Antonios Kelarakis

Received: 17 October 2024
Revised: 11 November 2024
Accepted: 17 November 2024
Published: 18 November 2024

Copyright: © 2024 by the authors. Licensee MDPI, Basel, Switzerland. This article is an open access article distributed under the terms and conditions of the Creative Commons Attribution (CC BY) license (https://creativecommons.org/licenses/by/4.0/).

1. Introduction

As a harmful air pollutant, nitrogen dioxide (NO_2) has been responsible for significant environmental issues, including acid rain and photochemical smog, which pose serious risks to human health [1,2]. Therefore, the on-line and real-time monitoring of NO_2 leakage is crucial for protecting both public health and environmental safety. The development of energy-efficient, sensitive, and reliable gas sensors for monitoring NO_2 concentrations has obtained considerable attention in recent years [3–5]. Metal oxides are well known for their excellent adsorption capacity, catalytic activity, and thermodynamic stability and are widely utilized in gas sensor applications [6]. Numerous metal oxides have been investigated as potential gas sensors, including ZnO, SnO_2, In_2O_3, WO_3, Fe_2O_3, and TiO_2 [6–12]. However, the performance of NO_2 gas sensors based on metal oxides remains unsatisfactory due to several limitations, such as high operating temperatures, elevated energy consumption, and poor reproducibility [13,14]. Notably, most metal oxide gas sensors require operation at high temperatures ranging from 200 to 400 °C. This not only makes them unsuitable for detecting gases that may contain explosive substances but also poses cost challenges for commercial applications. The prolonged response and recovery times, along with the low sensitivity at room temperature, represent significant bottlenecks for the practical

applicability of TiO_2-based gas sensors. To address these issues, it is essential to incorporate or integrate TiO_2 with hybrid nanocomposite materials such as graphene compounds and metal nanoparticles. This approach has been widely regarded as an effective strategy to enhance gas sensing performance.

Due to the introduction of oxygen functional groups and surface defects that serve as active sites for gas adsorption, graphene oxide (GO) and reduced graphene oxide (rGO) are increasingly recognized as suitable materials for room temperature gas sensing [15]. However, due to the limitations in gas sensor fabrication associated with the low defect density of graphene, numerous researchers have sought to develop gas sensors utilizing reduced graphene oxide (rGO), which possesses a higher defect density [16,17]. The development of low cost, transparent, and flexible rGO-based sensors for detecting harmful gases at very low concentrations is significantly important yet still challenging [18]. The TiO_2 nanoparticles/reduced graphene oxide (TiO_2 NPs/rGO) composite demonstrated a significant gas response (~14.9%), which is 4.57 times higher than that of pristine counterparts, along with excellent selectivity, high sensitivity, rapid response and recovery times, as well as remarkable repeatability towards nitrogen dioxide (NO_2) at a concentration of 100 ppm at room temperature [19]. The anti-humidity sensing performance of Pt/GO/TiO_2 is improved by increasing the thickness of the GO interlayer. Remarkably, the diode with a GO areal loading of 0.969 mg cm^{-2} exhibits a response retention rate ($R_{RH95\%}/R_{dry}$) of nearly 100% at 298 K [20]. A variety of high-performance and low-temperature gas sensors based on rGO hybrids have been reported. A straightforward one-pot microwave-assisted hydrothermal method has been employed to synthesize SnO_2/rGO composites, resulting in a significant reduction in the response and recovery times from 39.2/54.7 min to just 6.5/1 min, with an impressive detection limit as low as 50 ppb [21]. Under UV irradiation from an LED, a sensor utilizing graphene/TiO_2 nanoparticles demonstrated a detection limit of approximately 50 ppb for NO_2 at room temperature [22]. NO_2 gas sensors based on a ZnO-rGO hybrid showed improved sensitivity and faster response and recovery times [23]. Furthermore, a low-operating-temperature NO_2 gas sensor based on rGO/SnS_2 has shown remarkable selectivity and reversibility towards NO_2, achieving a low detection limit of 0.6 ppm with a response rate of 9.8% at 80 °C [24]. Moreover, when exposed to 1 ppm NO_2 at room temperature, CuO/rGO hybrids displayed a sensitive response quantified at around 14 [25].

In this manuscript, we fabricated a highly efficient room temperature NO_2 sensor utilizing TiO_2 nanotubes/reduced graphene oxide (TiO_2 NTs/rGO) nanocomposites. In addition, the fabricated gas sensor exhibits a highly sensitive response and excellent selectivity towards NO_2 gas, and the mechanism underlying the gas sensing performance was also investigated.

2. Experimental Details

2.1. Synthesis of Materials

All chemical reagents were of analytical grade (Beijing Chemical Co., Ltd., Beijing, China) and utilized without further purification. TiO_2 nanotube arrays were synthesized through the anodization of titanium foil (99.99%) at a voltage of 45 V for a duration of 2 h. The electrolyte was composed of ethylene glycol (99.99%), 0.3 M ammonium fluoride (NH_4F, 99%), and 2 vol% water (H_2O). Following anodization, the samples were annealed at 400 °C for 2 h, after which they were sonicated for 30 min and subjected to another round of annealing for 2 h. Then, the samples were removed from the bath and allowed to dry at room temperature for 1 h before being further annealed at 600 °C for 2 h in a furnace under air atmosphere. Subsequently, the samples were immersed in a solution containing 3-aminopropyl triethoxysilane and ethanol, followed by refluxing at 80 °C for 2 h. The TiO_2 nanotubes were then thoroughly rinsed with ethanol and deionized water before being dried at room temperature. The reduction of graphene oxide (GO) into reduced graphene oxide (rGO) was accomplished by exposing GO suspension to UV radiation for 1 h. The electrostatic interaction between positively charged nanotubes and negatively charged rGO

facilitates the adhesion of graphene derivatives onto the surface of the nanotubes [26]. The theoretical weight percentages of rGO within the TiO_2 NTs/rGO nanocomposites were calculated to be approximately 0.5 wt%, 1 wt%, and 3 wt%. For clarity, these TiO_2 NTs/rGO nanocomposites will henceforth be referred to as containing either 0.5 wt%, 1 wt%, or 3 wt% rGO in subsequent figures. Figure 1a displays a schematic of the synthesis process.

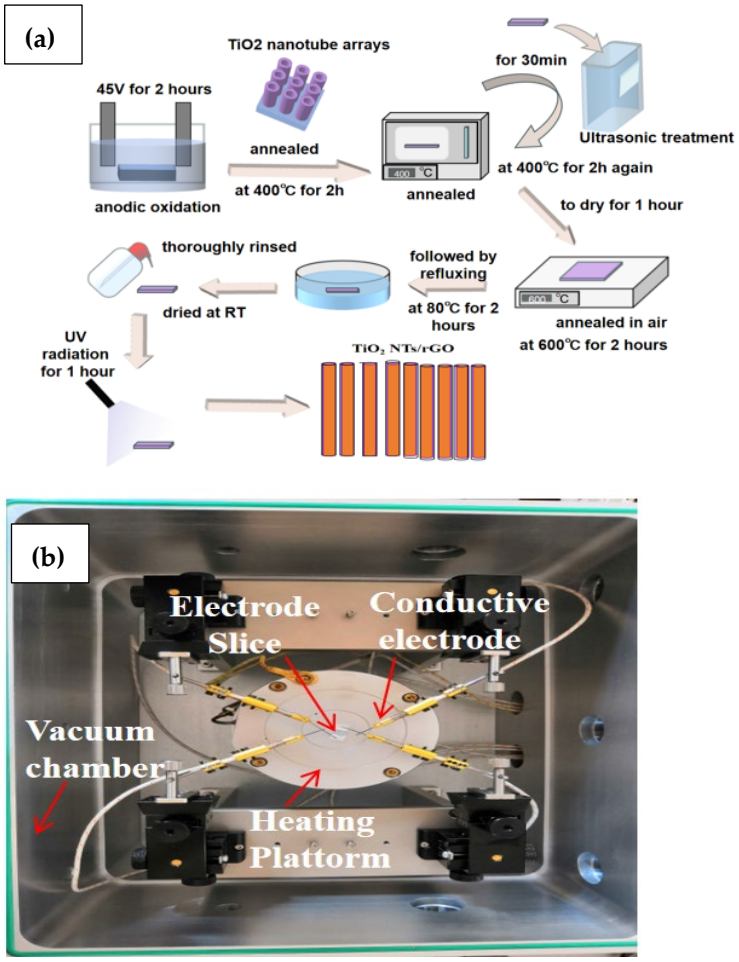

Figure 1. Schematic of synthesis process (**a**) and photograph of NO_2 detection testing system (**b**).

2.2. Characterization

The energy dispersive spectrometry (EDS) and field emission scanning electron microscopy (FESEM) images were acquired using a JEOL JSM-7500F microscope operating at 15 kV (JEOL, Japan). For the X-ray powder diffraction (XRD) analysis, we utilized X-ray diffractometer (XRD; D8, Karlsruhe, Germany) at a scanning rate of 0.02 s^{-1}. The Raman spectroscopy analysis was performed using the RENISHAW INVIA Micro-Raman spectrometer (Renishaw, UK). The X-ray photoelectron spectroscopy (XPS, Kratos XSAM800, Kratos Ltd., Manchester, Britain) was used to examine the chemical bonding states with Mg K_a excitation. Transmission electron microscopy (TEM) and high-resolution transmission electron microscopy (HR-TEM) were conducted on a JEOL JEM-2100F microscope operating at an accelerating voltage of 200 kV. The specific surface area was estimated using the Brunauer–Emmett–Teller (BET) (BET, 3H-2000ps4, China) equation based on nitrogen adsorption isotherms, following prior degassing of the sample under vacuum at 120 °C.

2.3. Fabrication and Measurement of the Gas Sensor

The photograph and structure of the NO_2 detection equipment are presented in Figure 1b [27,28]. The fabrication process can be described as follows: First, a suitable amount of the as-grown TiO_2 NTs/rGO powder was thoroughly mixed with deionized

water to create homogeneous slurry. This slurry was then carefully coated onto an alumina tube using a small brush to form a sensing film. A pair of Au electrodes was installed at each end of the tube, with each electrode connected to a pair of Pt wires. After allowing it to dry in air at room temperature, the device underwent annealing at 200 °C for 2 h to eliminate any residual water. Finally, a Ni-Cr alloy coil was inserted into the alumina ceramic tube to serve as a heater. The operating temperature is controlled by adjusting the heating current supplied to the ceramic heater. The response of the sensor is defined as $S = R_g/R_a$, where R_a and R_g represent the electrical resistance of the gas sensor in air and in NO_2, respectively. The response time or recovery time was defined as the time taken for 90% resistance variation.

3. Results and Discussion

3.1. Structural and Morphological Characteristics

Figure 2 presents the XRD patterns of the TiO_2 NTs/rGO nanocomposites synthesized with varying rGO contents. The XRD pattern for undoped TiO_2 nanotubes displays very sharp diffraction peaks, all of which can be confidently assigned to the anatase TiO_2 phase (JCPDS Card No. 21-1272). It is important to note that the incorporation of reduced graphene oxide does not alter the original crystal structure of TiO_2. All diffraction peaks in the nanocomposites are observed at nearly identical 2θ positions when compared to those of undoped TiO_2. However, with an increase in rGO doping, there is a noticeable decrease in the intensity of the diffraction peaks for TiO_2 NTs/rGO nanocomposites, which can be attributed to an excess formation of nucleation centers [29]. Additionally, it is interesting to observe from the XRD pattern of TiO_2 NTs/rGO with an rGO content of 3 wt.% that a weak peak appears between 23° and 26°, which corresponds to the (002) plane of rGO [30,31].

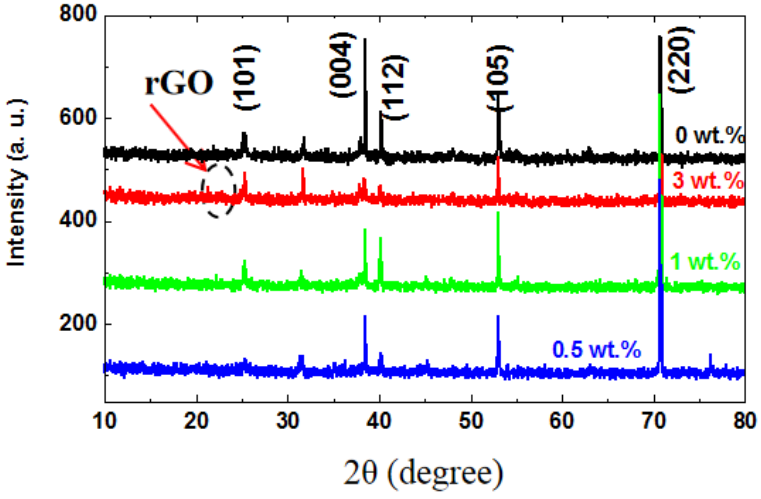

Figure 2. XRD patterns of TiO_2 NTs/rGO nanocomposites grown with different rGO contents.

As illustrated in Figure 3a, the TiO_2 nanotubes are characterized by vertically arranged structures with an average diameter ranging from approximately 80 to 120 nm. For the TiO_2 NTs/rGO nanocomposites with rGO concentrations of 0.5 and 1 wt.%, graphene sheets are not distinctly visible in Fig. 3b and 3c. However, for those with rGO contents of 3 wt.%, it is evident that the rGO sheets not only partially surround the TiO_2 nanotubes but also establish interconnection bridges between adjacent nanotubes (Figure 3d). This connectivity through the rGO layer is anticipated to enhance electron–hole separation by facilitating electron transfer from TiO_2. In addition, electrons traveling along the graphene layer may interact with adsorbed NO_2 molecules as well. To confirm the presence of graphene within these composites, we conducted an EDS analysis on samples with a rGO content of 3 wt.%. The EDX spectrum presented in the inset of Figure 3d reveals peaks corresponding to titanium (Ti), oxygen (O), and carbon (C) elements.

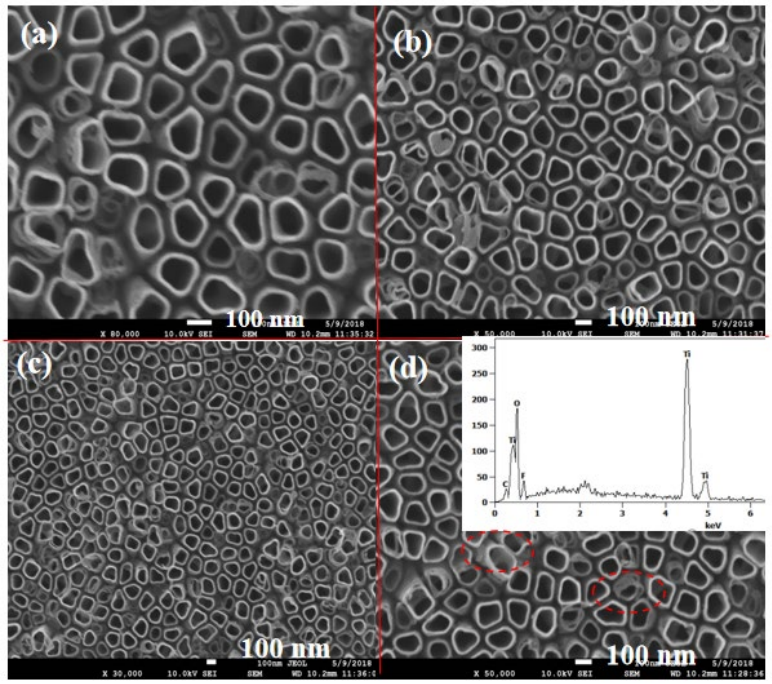

Figure 3. SEM images of TiO_2 NTs/rGO nanocomposites with rGO contents of 0 wt.% (**a**), 0.5 wt.% (**b**), 1 wt.% (**c**), and 3 wt.% (**d**), respectively. Inset of Figure 3d shows the EDX spectrum of TiO_2 NTs/rGO nanocomposites with rGO contents of 3 wt.%. The red circles in Figure 3d illustrate the structure of rGO surrounding the TiO_2 nanotubes.

As can be seen in the TEM images shown in Figure 4a,b, there is no significant difference in diameter and length between TiO_2 nanotubes and TiO_2 NTS/rGO nanocomposites. To gain deeper insights into the nature of the interface, we conducted HR-TEM analysis, with the corresponding image presented in Figure 4d. When compared to the undoped TiO_2 nanotubes shown in Figure 4c, it becomes evident that thin layers are wrapped around the outer surface of the TiO_2 nanotubes, indicating successful modification by rGO. The observed lattice spacing of 0.35 nm for the TiO_2 nanotubes corresponds to the (110) orientation of anatase phase TiO_2. The layer material in contact with TiO_2 is rGO, which forms a close-contact interface with the surface of these nanotubes, which is believed to facilitate electron transmission. However, it is important to note that any observed inhomogeneity within the nanocomposites may arise from limitations associated with chemical processes or reaction times, or the sample preparation method for TEM.

3.2. Raman and XPS Characteristics

The Raman spectra of TiO_2 NTs/rGO nanocomposites, as illustrated in Figure 5, reveal two prominent peaks corresponding to the D and G bands of graphene. The G band provides valuable information regarding the in-plane vibrations of sp^2 bonded carbon atoms [32], while the D band is associated with some sp^3 defects present in rGO [33]. The characteristics of Raman modes of anatase phase appeared at 146, 400, 518, and 636 cm^{-1} for pristine TiO_2, and these peaks are well matched with E_g, B_{1g}, A_{1g} + B_{1g}, and Eg modes of the anatase TiO_2 phase [34]. As depicted in Figure 5, the G band for TiO_2 NTs/rGO composites appears at 1597 cm^{-1}, which is quite close to that of pristine graphene (1580 cm^{-1}). The slight red shift observed in the G band for TiO_2 NTs/rGO nanocomposites compared to GO (1591 cm^{-1}) suggests a restoration of the π-π systems within graphene during the chemical reaction. Additionally, it is widely recognized that the I_D/I_G ratio serves as a valuable indicator of crystal quality within graphite structures. Our calculations indicate that the I_D/I_G ratio for 3 wt.% TiO_2 NTs/rGO (1.26) exceeds that of 0.5 wt.% TiO_2 NTs/rGO (1.14), signifying a stronger D band signal and thus confirming successful

incorporation of rGO into these nanocomposites. Additionally, spectral characteristics suggest an increase in defect point density on the resulting rGO sheets, which may serve as ideal adsorption–desorption sites for TiO_2 nanotubes [31].

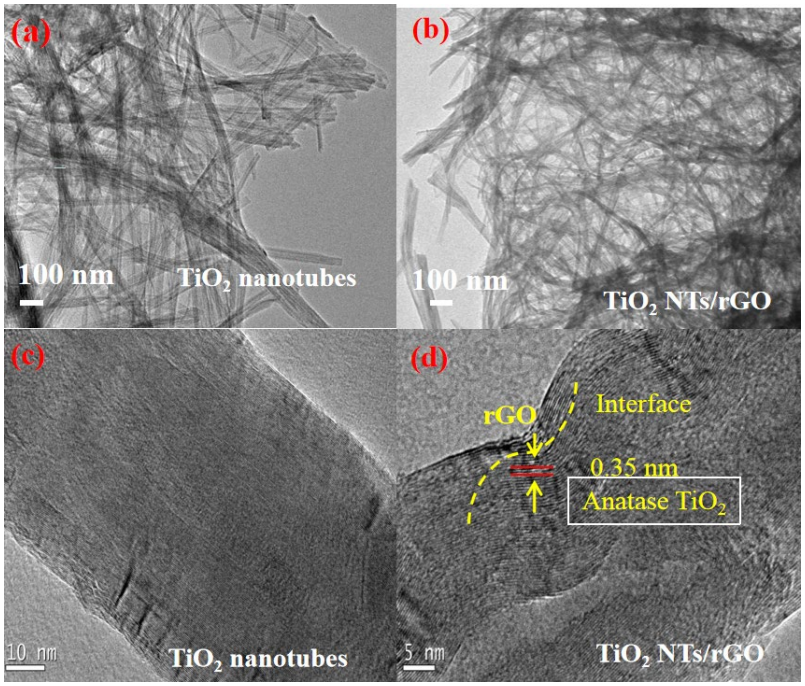

Figure 4. TEM (**a**,**b**) and high-resolution TEM (**c**,**d**) images of TiO_2 nanotubes (**a**,**c**) and TiO_2 NTs/rGO nanocomposites (**b**,**d**) with rGO contents of 1 wt.%.

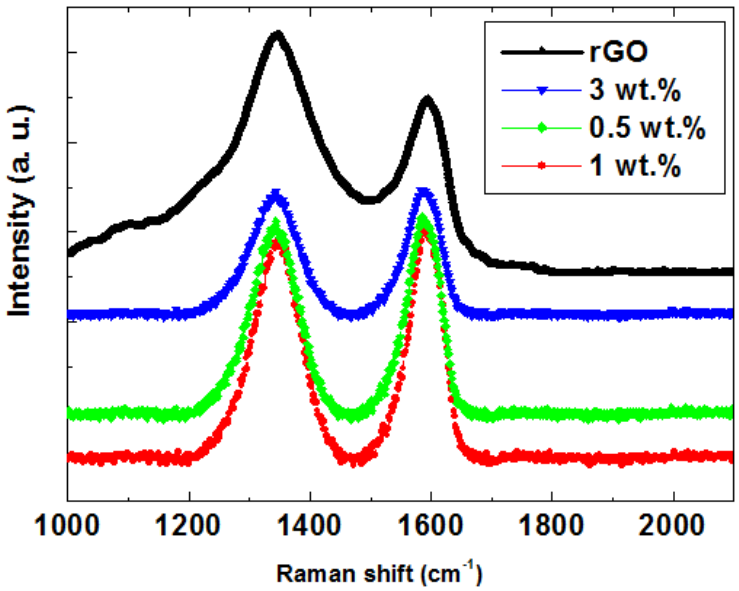

Figure 5. Raman spectra of TiO2 NTs/rGO nanocomposites with different rGO contents.

The chemical states of the elements were carefully analyzed using XPS and are illustrated in Figure 6. The sharp peaks observed in the full scan spectra indicate a clear presence of C, O, and Ti elements for TiO_2 NTs/rGO nanocomposites. The TiO_2 NTs/rGO nanocomposite with a rGO content of 1 wt.% exhibits the best gas sensing performance. Therefore, we selected this sample for XPS characterization. In Figure 6b, the Ti $2p_{3/2}$ and Ti $2p_{1/2}$ peaks are located at binding energies of 458.9 and 464.8 eV, which correspond to

the values for Ti^{4+} in TiO_2 [35]. As shown in Figure 6c, the high-resolution C 1s peak was accurately fitted with three distinct components. The binding energy at 284.3 eV, 285.1 eV, and 287.5 eV can be attributed to C-C bonds (sp^2 hybridized carbon) from rGO, C-O-Ti bonds and O-C=O species, respectively [36]. The fitted peak at 285.1 eV corresponding to the C-O-Ti bond further confirms that a chemically bonded heterostructure has indeed formed between TiO_2 NTs and rGO [37]. This heterostructure facilitates close contact between TiO_2 nanotubes and rGO, thereby promoting effective electron transfer. In Figure 6d, we present the high-resolution XPS spectrum for O 1s, which can be resolved into three Gaussian peaks representing different types of oxygen species. The three peaks can be respectively attributed to oxygen vacancy in defective TiO_2, lattice oxygen species (Ti-O bands), and chemisorbed or dissociated oxygen species (C=O) [38]. The increase in oxygen vacancies within defective TiO_2 suggests that there are more active sites available in the TiO_2 NTS/rGO nanocomposites, which is advantageous for gas adsorption and reaction. Additionally, the rise in C=O bonds in these nanocomposites indicates that the oxygen species adsorbed on the surface can participate effectively in surface redox reactions, leading to significant changes in sensor resistance. Therefore, by incorporating rGO, the TiO_2 NTs/rGO nanocomposite demonstrates a remarkable ability to adsorb ionized oxygen, contributing to its potential for high-performance gas sensing applications [39].

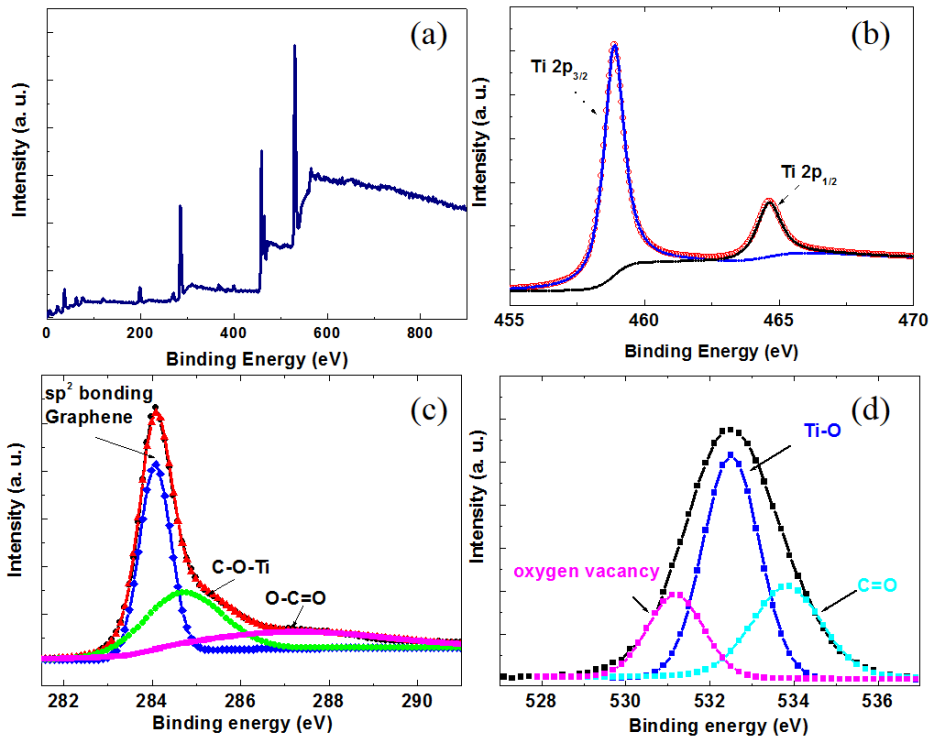

Figure 6. XPS spectra of TiO_2 NTs/rGO nanocomposite with rGO contents of 1 wt.%. (**a**) Full scan. (**b**) Ti 2p. (**c**) C 1s. (**d**) O 1s.

3.3. Gas Sensing Properties

The relationship between the response and NO_2 concentration for the sensor based on TiO_2 NTs/rGO nanocomposites at room temperature is illustrated in Figure 7. It can be observed that the response increases with NO_2 concentration, ranging from 1 ppm to 50 ppm. Notably, the TiO_2 NTs/rGO nanocomposite with contents of 1.0 wt.% exhibited the highest response value, reaching an impressive 138 at a NO_2 concentration of 50 ppm. The limit of detection was determined to be 1 ppm, and it is worth mentioning that the sensor demonstrated a remarkable response of 19.1 for just 1 ppm NO_2 when utilizing the TiO_2 NTs/rGO composite with rGO contents of 1.0 wt.%.

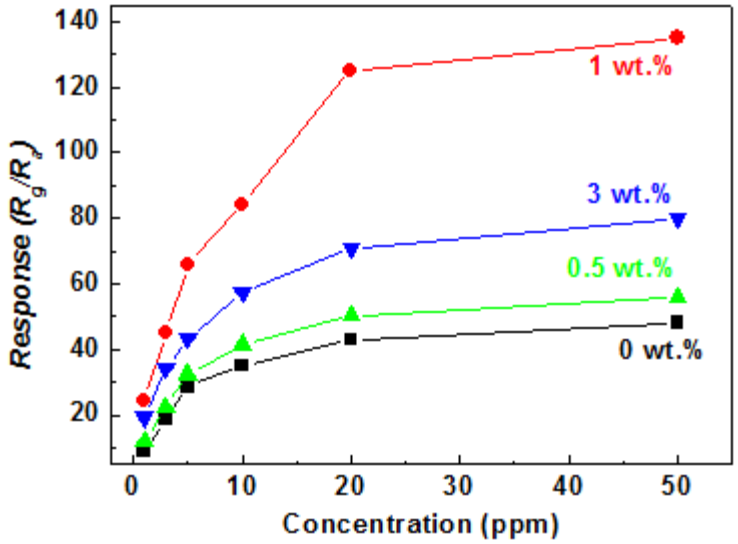

Figure 7. The response value of the sensor based on TiO_2 NTs/rGO composites vs. NO_2 concentration at room temperature.

The response and recovery curves of the sensor to 20 ppm NO_2 are presented in Figure 8. The calculated response/recovery times are as follows: 24 s/42 s for TiO_2 nanotubes, 23 s/34 s for TiO_2 NTs/rGO (0.5 wt.%), 18 s/33 s for TiO_2 NTs/rGO (1 wt.%), and 20 s/35 s for TiO_2 NTs/rGO (3 wt.%). It is evident that the sensors based on the 1 wt.% rGO doped TiO_2 NTs/rGO exhibit a significantly faster response time. However, it is worth noting that the response time tends to increase with higher doping amounts of rGO. The relative filling and partial binding of TiO_2 nanotubes due to rGO doping positively influence gas permeation into the sensing layer as well as electron transfer from TiO_2 to graphene, which may contribute to a quicker reduction in resistance. Nevertheless, an increase in rGO doping can lead to agglomeration, which reduces the active sites available for gas molecules and consequently diminishes resistance charge. The room temperature NO_2 gas sensing performances of TiO_2 NTs/rGO were compared with previous metal-semiconductor oxide/rGO nanocomposites. In Table 1, we can see that in low concentration detection and response/recovery time, TiO_2 NTs/rGO exhibited better gas sensing performance than most of the previously reported composites.

Table 1. Comparison of the RT NO_2 gas sensing performances of our device with those reported in previous literature.

Ref.	Device Structure	Target Gas	Working Temperature (°C)	Response (%)/ppm	Response/Recovery Time (s)
[3]	rGO/CeO_2	NO_2	RT	8.2/25	180/260
[4]	In_2O_3/rGO	NO_2	RT	8.25/30	165/235
[5]	Graphene/ZnO	NO_2	300	9.5/50	145/248
[40]	TiO_2 NPs/rGO	NO_2	RT	14.9/100	124/182
This work	TiO_2 NTs/rGO	NO_2	RT	19.1/1	18 s/33 s

The selectivity of gas sensors is another crucial parameter for real-time applications. As illustrated in Figure 9, the sensor utilizing TiO_2 NTs/rGO composites (1 wt. %) demonstrated an impressive response to NO_2, with its value being at least four times greater than that observed for other test gases. This behavior regarding CO, H_2S, and H_2 can be attributed to the low operating temperature and relatively low concentration of the

detected gases [41]. Based on these findings, it is evident that the sensor employing TiO_2 NTS/rGO nanocomposites exhibits superior performance in detecting low concentrations of NO_2 at lower temperatures compared to other detection gases.

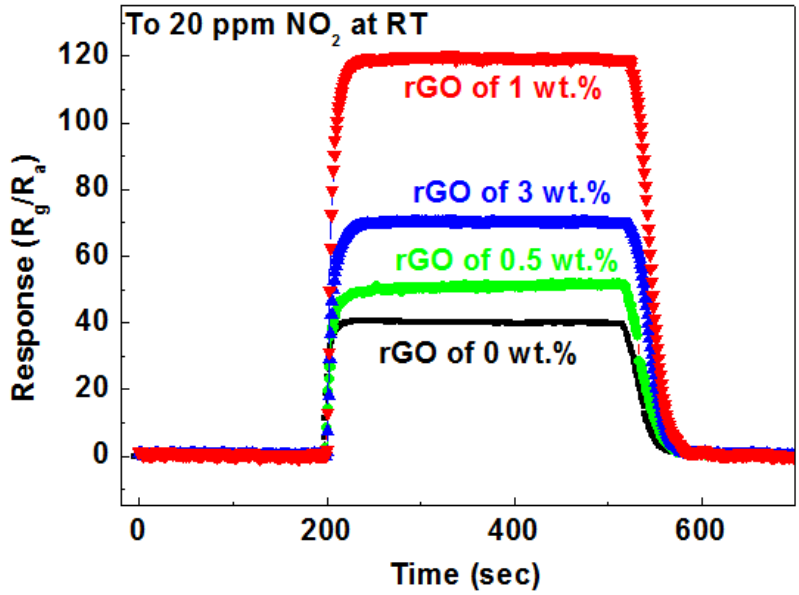

Figure 8. The dynamic response transients of the sensor based on TiO_2 NTs/rGO nanocomposites to 20 ppm NO_2 at room temperature.

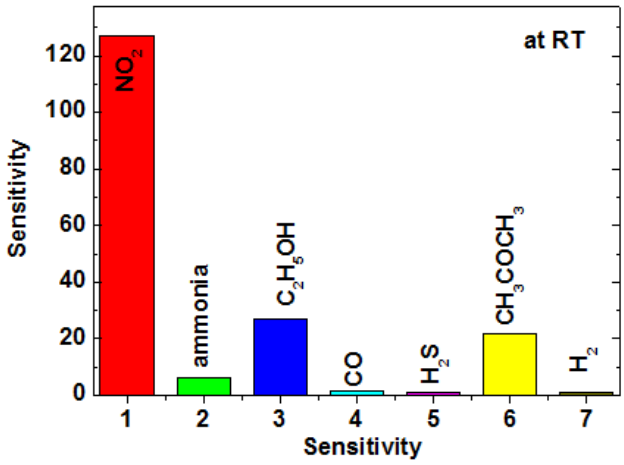

Figure 9. Response of the sensor based on TiO_2 NTs/rGO nanocomposites to 50 ppm of C_2H_5OH, CH_3OH, H_2, NH_3, H_2S, and NO_2 at room temperature.

The repeatability and long-term stability of the sensor were investigated, providing crucial parameters for practical applications. The long-term stability of the sensors based on TiO_2 nanotubes (NTs) and TiO_2 NTs/reduced graphene oxide (rGO) nanocomposites in response to 1 ppm NO_2 at room temperature is illustrated in Figure 10. The sensor utilizing TiO_2 NTs/rGO (1 wt.%) exhibited a stable response of 17.2 (17.2 $\pm$ 0.3) for 1 ppm NO_2 at room temperature, demonstrating excellent long-term stability.

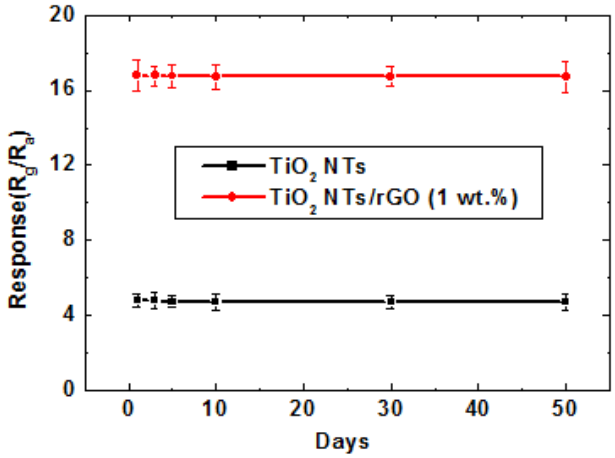

Figure 10. Long-term stability of the sensor based on TiO_2 NTs and TiO_2 NTs/rGO nanocomposites to 1 ppm of NO_2 at room temperature.

3.4. Gas Sensing Mechanism of TiO_2 NTs/rGO Nanocomposites

The sensing principle of resistance is fundamentally based on the changes in sensor resistance, which occurs due to variations in charge carriers and is closely linked to the amount of chemically adsorbed substances present on the surface of metal oxides. In the case of *n-type* TiO_2, O_2 molecules from the atmosphere are adsorbed onto its surface and subsequently transform into O^-, O_2^-, and O^{2-} by capturing electrons from TiO_2. However, when NO_2 is introduced, its chemical adsorption further reduces conductivity through an electron capture effect. We have observed that incorporating rGO can significantly enhance the conductivity of these sensors, thereby improving their gas sensing performance at room temperature. As illustrated by the I-V curves shown in Figure 11, it becomes evident that the TiO_2 NTs/rGO nanocomposite exhibits much lower resistance compared to undoped TiO_2 nanotubes, which indicates a notable improvement in charge transfer performance. Moreover, with an increase in active sites such as vacancies, defects, and oxygen functional groups, we expect a significant improvement in both the gas adsorption and diffusion rates of NO_2 molecules on these active surfaces.

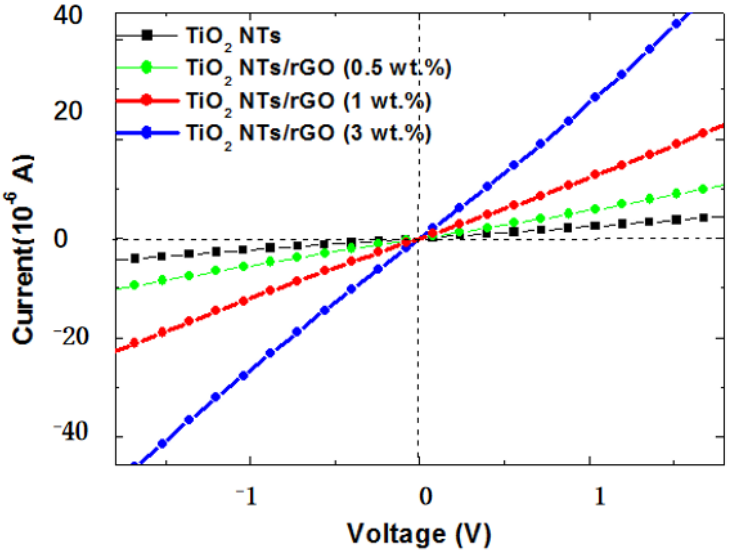

Figure 11. I-V curves of the sensor based on TiO_2 NTs/rGO nanocomposites with different rGO contents.

Another mechanism contributing to the enhancement of the sensor can be attributed to the formation of a *p-n* heterojunction between *n-type* TiO_2 and *p-type* rGO. The close contact between these two distinct semiconductor materials allows for the alignment of

their Fermi energy levels at the interface, which typically results in charge transfer and the establishment of a charge depletion layer. Figure 12a illustrates the energy band diagrams for TiO_2 nanotubes, rGO, and their corresponding TiO_2 NTs/rGO nanocomposites. The work function for TiO_2 NTs is approximately 5.1 eV, while that of rGO is around 4.42 eV. Upon forming the TiO_2/rGO heterojunction, an electron accumulation region develops on the surface of TiO_2 NTs. This charge transfer creates a potential barrier at the heterojunction, leading to bending in both vacuum energy levels and energy bands. The initial electron transfer from TiO_2 to graphene generates a surface depletion region on TiO_2, resulting in increased resistance. In ambient air conditions, where no barriers exist between TiO_2 NTs and graphene, electrons can flow freely from TiO_2 NTs to graphene. However, upon exposure to NO_2 gas, there is an increase in potential barrier height at the interfaces between *n-type* TiO_2 NTs and *p-type* rGO, which makes electron transfer from *p-type* graphene to *n-type* TiO_2 NTs more challenging and ultimately leads to an increase in sensor resistance (Figure 12b).

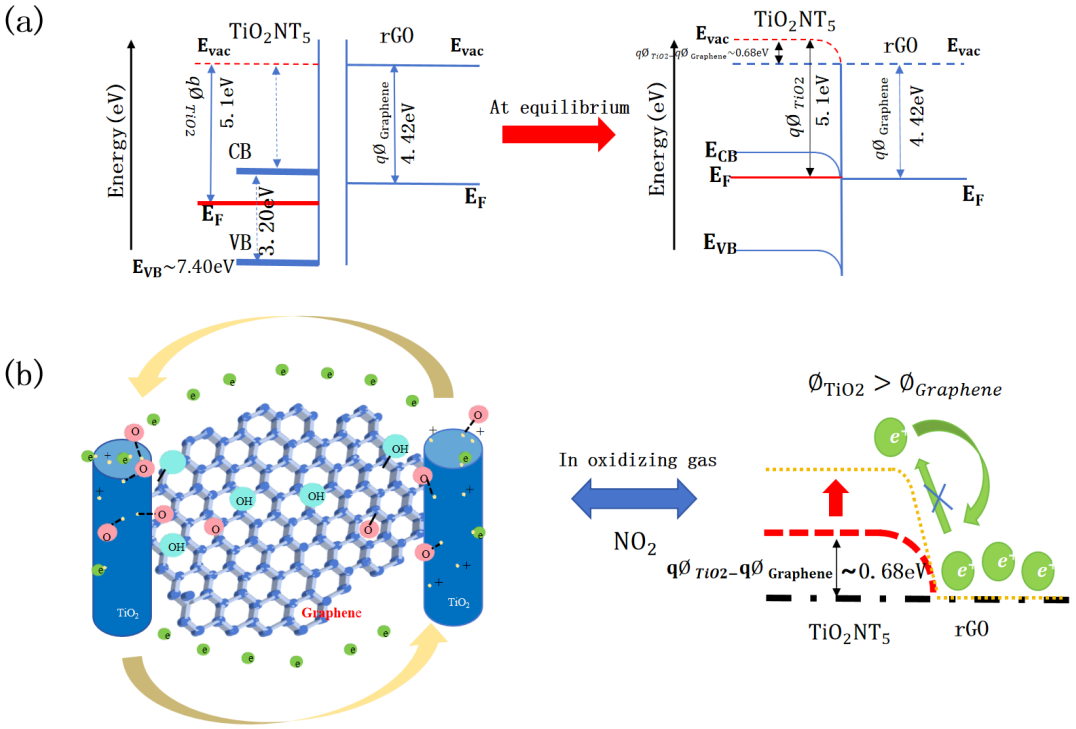

Figure 12. Energy band diagrams for TiO_2 NTs, rGO and TiO_2 NTs/rGO heterostructure, where E_{VB}, E_F, E_{CB}, E_{vac} represent valence band, Fermi level, conduction band, and vacuum level, respectively. (**a**) The energy band diagrams for TiO_2 nanotubes, rGO, and their corresponding TiO_2 NTs/rGO nanocomposites. (**b**) Schematic illustration of electron transfer and sensing mechanism of TiO_2 NTs/rGO nanocomposites.

4. Conclusions

In summary, TiO_2 nanotube arrays modified by rGO nanosheets were successfully synthesized using a straightforward two-step method. The SEM images reveal that the rGO layer not only partially enveloped the TiO_2 nanotubes but also established a close connection between adjacent nanotubes, thereby enhancing the efficiency of electron–hole separation. The gas sensing properties of the TiO_2 NTs/rGO nanocomposites demonstrated high sensitivity to NO_2 at low operating temperatures, characterized by an enhanced response, relatively short recovery time, and excellent selectivity. The improved gas sensing performance can be attributed to the formation of a *p-n* heterojunction between *n-type* TiO_2 and *p-type* rGO. Furthermore, due to the presence of rGO sheets, the rate of gas adsorption and diffusion on the active surface of TiO_2 NTs/rGO nanocomposites was significantly facilitated by an increased number of active sites.

Author Contributions: Methodology, Y.Y. and C.T.; Investigation, Y.L., C.T. and C.Z.; Data curation, Y.L. and C.T.; Writing—original draft, Y.L., Y.Y. and C.Z. All authors have read and agreed to the published version of the manuscript.

Funding: This research was funded by the Innovation team project of Lingnan Normal University (LT2203), Science and Technology Project of Zhanjiang (2019A03009, 2022A01001, 2023A21510), and Natural Science Foundation of Guangdong Province (2022A1515011137, 2023A1515011796, 2023A1515012923).

Data Availability Statement: Data are contained within the article.

Conflicts of Interest: The authors declare no conflict of interest.

References

1. Deng, S.; Tjoa, V.; Fan, H.M.; Tan, H.R.; Sayle, D.C.; Olivo, M.; Mhaisalkar, S.; Wei, J.; Sow, C.H. Reduced graphene oxide conjugated Cu2O nanowire mesocrystals for high-performance NO2 gas sensor. *J. Am. Chem. Soc.* **2012**, *134*, 4905–4917. [CrossRef] [PubMed]
2. Turlybekuly, A.; Sarsembina, M.; Mentbayeva, A.; Bakenov, Z.; Soltabayev, B. CuO/TiO_2 heterostructure-based sensors for conductometric NO_2 and N_2O gas detection at room temperature. *Sens. Actuators B* **2023**, *397*, 134635. [CrossRef]
3. Hu, J.; Zou, C.; Su, Y.; Li, M.; Ye, X.; Cai, B.; Kong, E.S.; Yang, Z.; Zhang, Y. Light-assisted recovery for a highly-sensitive NO_2 sensor based on RGO-CeO_2 hybrids. *Sens. Actuators B Chem.* **2018**, *270*, 119–129. [CrossRef]
4. Gu, F.; Nie, R.; Han, D.; Wang, Z. In_2O_3–graphene nanocomposite based gas sensor for selective detection of NO_2 at room temperature. *Sens. Actuators B Chem.* **2015**, *219*, 94–99. [CrossRef]
5. Kim, H.W.; Kwon, Y.J.; Mirzaei, A.; Kang, S.Y.; Choi, M.S.; Bang, J.H.; Kim, S.S. Synthesis of zinc oxide semiconductors-graphene nanocomposites by microwave irradiation for application to gas sensors. *Sens. Actuators B Chem.* **2017**, *249*, 590–601. [CrossRef]
6. Young, S.-J.; Chu, Y.-L. Hydrothermal Synthesis and Improved CH_3OH-Sensing Performance of ZnO Nanorods with Adsorbed Au NPs. *IEEE Trans. Electron Devices* **2021**, *68*, 1886–1891. [CrossRef]
7. Chu, Y.-L.; Young, S.-J.; Ji, L.-W.; Chu, T.-T.; Lam, K.-T.; Hsiao, Y.-J.; Tang, I.-T.; Kuo, T.-H. Characteristics of Gas Sensors Based on Co-Doped ZnO Nanorod Arrays. *J. Electrochem. Soc.* **2020**, *167*, 117503. [CrossRef]
8. Zhang, D.H.; Liu, Z.Q.; Li, C.; Tang, T.; Liu, X.L.; Han, S.; Lei, B.; Zhou, C.W. Detection of NO_2 down to ppb levels using individual and multiple In_2O_3 nanowire devices. *Nano Lett.* **2004**, *4*, 1919–1924. [CrossRef]
9. Tsai, Y.T.; Chang, S.J.; Ji, L.W.; Hsiao, Y.J.; Tang, I.T.; Lu, H.Y.; Chu, Y.L. High Sensitivity of NO Gas Sensors Based on Novel Ag-Doped ZnO Nanoflowers Enhanced with a UV Light-Emitting Diode. *ACS Omega* **2018**, *3*, 13798–13807. [CrossRef]
10. Wetchakun, K.; Samerjai, T.; Tamaekong, N.; Liewhiran, C.; Siriwong, C.; Kruefu, V.; Wisitsoraat, A.; Tuantranont, A.; Phanichphant, S. Semiconducting metal oxides as sensors for environmentally hazardous gases. *Sens. Actuators B-Chem.* **2011**, *160*, 580–591. [CrossRef]
11. Young, S.-J.; Chu, Y.-L. Platinum Nanoparticle-Decorated ZnO Nanorods Improved the Performance of Methanol Gas Sensor. *J. Electrochem. Soc.* **2020**, *167*, 147508. [CrossRef]
12. Qin, Y.; Zhang, X.; Wang, Y. Remarkable improvement of $W_{18}O_{49}/TiO_2$ heteronanowires in ambient temperature-responsive NO_2-sensing abilities and its unexpected n-p transition phenomenon. *Sens. Actuators B* **2017**, *240*, 477–486. [CrossRef]
13. Korotcenkov, G. The role of morphology and crystallographic structure of metal oxides in response of conductometric-type gas sensors. *Mater. Sci. Eng. R* **2008**, *61*, 1–39. [CrossRef]
14. Sun, F.Q.; Cai, W.P.; Li, Y.; Jia, L.C.; Lu, F. Direct growth of mono- and multilayer nanostructured porous films on curved surfaces and their application as gas sensors. *Adv. Mater.* **2005**, *17*, 2872–2877. [CrossRef]
15. Yuan, W.J.; Liu, A.R.; Huang, L.; Li, C.; Shi, G.Q. High-performance NO_2 sensors based on chemically modified graphene. *Adv. Mater.* **2013**, *25*, 766–771. [CrossRef]
16. Jung, M.W.; Kang, S.M.; Nam, K.H.; An, K.S.; Ku, B.C. Highly transparent and flexible NO_2 gas sensor film based on MoS_2/rGO composites using soft lithographic patterning. *Appl. Suf. Sci.* **2018**, *456*, 7–12. [CrossRef]
17. Liu, X.; Sun, J.B.; Zhang, X.T. Novel 3D graphene aerogel-ZnO composites as efficient detection for NO_2 at room temperature. *Sens. Actuators B* **2015**, *211*, 220–226. [CrossRef]
18. Varghese, S.S.; Lonkar, S.; Singh, K.K.; Swaminathan, S.; Abdala, A. Recent advances in graphene based gas sensors. *Sens. Actuat. B Chem.* **2015**, *218*, 160–183. [CrossRef]
19. Murali, G.; Reddeppa, M.; Seshendra Reddy, C.; Park, S.; Chandrakalavathi, T.; Kim, M.D.; In, I. Enhancing the charge carrier separation and transport via nitrogen-doped graphene quantum dot-TiO_2 nanoplate hybrid structure for an efficient NO gas sensor. *ACS Appl. Mater. Interfaces* **2020**, *12*, 13428–13436. [CrossRef]
20. Li, R.; Xu, Z.; Mao, B.; Xie, G.; Wang, Y.; Liu, Z.; Fang, H. Pt/GO/TiO_2 room-temperature hydrogen sensing Schottky diode: High resistance to humidity interference endowed by the graphene oxide interlayer. *Sens. Actuators B Chem.* **2024**, *408*, 135569. [CrossRef]
21. Wang, Z.; Jia, Z.; Li, Q.; Zhang, X.; Sun, W.; Sun, J.; Liu, B.; Ha, B. The enhanced NO_2 sensing properties of SnO_2 nanoparticles/reduced graphene oxide composite. *J. Colloid Interface Sci.* **2019**, *537*, 228–237. [CrossRef] [PubMed]

22. Giampiccolo, A.; Tobaldi, D.M.; Leonardi, S.G.; Murdoch, B.J.; Seabra, M.P.; Ansell, M.P.; Neri, G.; Ball, R.J. Sol gel graphene/TiO_2 nanoparticles for the photocatalytic-assisted sensing and abatement of NO_2. *Appl. Catal. B Environ.* **2019**, *243*, 183–194. [CrossRef]
23. Liu, S.; Yu, B.; Zhang, H.; Fei, T.; Zhang, T. Enhancing NO_2 gas sensing performances at room temperature based on reduced graphene oxide-ZnO nanoparticles hybrids. *Sens. Actuators B Chem.* **2014**, *202*, 272–278. [CrossRef]
24. Shafiei, M.; Bradford, J.; Khan, H.; Piloto, C.; Wlodarski, W.; Li, Y.; Motta, N. Low-operating temperature NO_2 gas sensors based on hybrid two-dimensional SnS_2-reduced graphene oxide. *Appl. Surf. Sci.* **2018**, *462*, 330–336. [CrossRef]
25. Li, Z.; Liu, Y.; Guo, D.; Guo, J.; Su, Y. Room-temperature synthesis of CuO/reduced graphene oxide nanohybrids for high-performance NO_2 gas sensor. *Sens. Actuators B Chem.* **2018**, *271*, 306–310. [CrossRef]
26. Rambabu, Y.; Kumar, U.; Singhal, N.; Kaushal, M.; Jaiswal, M.; Jain, S.L.; Roy, S.C. Photocatalytic reduction of carbon dioxide using graphene oxide wrapped TiO_2 nanotubes. *Appl. Surf. Sci.* **2019**, *485*, 48–55. [CrossRef]
27. Wang, J.; Ke, L.; Wu, J.; Liang, F.; Xiang, Y. Research and Development of Online Monitoring Protection Sensors for Paper Books Based on TiO_2 NT/MoS_2. *Coatings* **2024**, *14*, 552. [CrossRef]
28. Wang, J.; Wang, Q.; He, S.; Chen, Z.; Qiu, W.; Yu, Y. Development and Application of a Nano-Gas Sensor for Monitoring and Preservation of Ancient Books in the Library. *Coatings* **2024**, *14*, 553. [CrossRef]
29. Lv, K.; Fang, S.; Si, L.; Xia, Y.; Ho, W.; Li, M. Fabrication of TiO_2 nanorod assembly grafted rGO (rGO@TiO_2-NR) hybridized flake-like photocatalyst. *Appl. Surf. Sci.* **2017**, *391*, 218–227. [CrossRef]
30. Zhang, X.Y.; Li, H.P.; Cui, X.L.; Lin, Y.H. Graphene/TiO_2 nanocomposites: Synthesis, characterization and application in hydrogen evolution from water photocatalytic splitting. *J. Mater. Chem.* **2010**, *20*, 2801–2806. [CrossRef]
31. Pimenta, M.A.; Dresselhaus, G.; Dresselhaus, M.S.; Cancado, L.G.; Jorio, A.; Saito, R. Studying disordering graphite-based systems by Raman spectroscopy. *Phys. Chem. Chem. Phys.* **2007**, *9*, 1276–1290. [CrossRef] [PubMed]
32. Zhang, W.; Cui, J.; Tao, C.; Wu, Y.; Li, Z.; Ma, L. A strategy for producing pure single-layer graphene sheets based on a confined self-assembly approach. *Angew. Chem. Int. Ed.* **2009**, *48*, 5848–5864. [CrossRef] [PubMed]
33. Moussa, S.; Panchakarla, L.S.; Ho, M.Q.; El-Shall, M.S. Graphene supported iron-based nanoparticles for catalytic production of liquid hydrocarbons from synthesis gas. *ACS Catal.* **2014**, *4*, 535–545. [CrossRef]
34. Saha, R.; Thukral, A.; Pal, A.; Saini, P. Sunlight responsive superhydrophilic rGO-TiO_2 nanocomposite coatings for photovoltaic applications. *Diam. Relat. Mater.* **2024**, *149*, 111603. [CrossRef]
35. Lin, Z.; Waller, G.; Liu, Y.; Liu, M.; Wong, C.P. Facile synthesis of nitrogen-doped graphene via pyrolysis of graphene oxide and urea, and its electrocatalytic activity toward the oxygen-reduction reaction. *Adv. Energy Mater.* **2012**, *2*, 884. [CrossRef]
36. Wang, C.; Xue, J.; Qiang, L.; Tang, J. A facile and efficient method to directly synthesize TiO_2/rGO with enhanced photocatalytic performance. *Superlattices Microstruct.* **2018**, *121*, 1–8.
37. Dong, F.; Guo, S.; Wang, H.; Li, X.; Wu, Z. Enhancement of the visible light photocatalytic activity of C-doped TiO_2 nanomaterials prepared by a green synthetic approach. *J. Phys. Chem. C* **2011**, *115*, 13285–13292. [CrossRef]
38. Perera, S.; Mariano, R.; Vu, K.; Nour, N.; Seitz, O.; Chabal, Y.; Balkus, K. Hydrothermal synthesis of graphene-TiO_2 nanotube composites with enhanced photocatalytic activity. *ACS Catal.* **2012**, *2*, 949–956. [CrossRef]
39. Niu, X.; Yan, W.; Zhao, H.; Yang, J. Synthesis of Nb doped TiO_2 nanotube/reduced graphene oxide heterostructure photocatalyst with high visible light photocatalytic activity. *Appl. Surf. Sci.* **2018**, *440*, 804–813. [CrossRef]
40. Harathi, N.; Bollu, M.; Pasupuleti, K.S.; Tauanov, Z.; Peta, K.R.; Kim, M.-D.; Reddeppa, M.; Sarkar, A.; Rao, V.N. PrGO decorated TiO_2 nanoplates hybrid nanocomposite for augmented NO_2 gas detection with faster gas kinetics under UV light irradiation. *Sens. Actuators B Chem.* **2022**, *358*, 131503. [CrossRef]
41. Maziarz, W. TiO_2/SnO_2 and TiO_2/CuO thin film nano-heterostructures as gas sensors. *Appl. Sur. Sci.* **2019**, *480*, 361–370. [CrossRef]

Disclaimer/Publisher's Note: The statements, opinions and data contained in all publications are solely those of the individual author(s) and contributor(s) and not of MDPI and/or the editor(s). MDPI and/or the editor(s) disclaim responsibility for any injury to people or property resulting from any ideas, methods, instructions or products referred to in the content.